J Fail. Anal. and Preven. (2018) 18:828–836
https://doi.org/10.1007/s11668-018-0470-0

TECHNICAL ARTICLE—PEER-REVIEWED

Failure Analysis of Insulator Iron Cap in Low Stress State

Xing Chen · Shuaijiang Yan · Chengsong Zhang · Guodong Cui · Chuan Yang

Submitted: 13 October 2017 / in revised form: 6 March 2018 / Published online: 26 April 2018
© ASM International 2018

Abstract The safe and stable operations of insulator components create an important issue, with massive constructions of high-voltage direct current (HVDC) projects. However, the service life of the insulator iron cap directly depends on the production process. Therefore, it is necessary to examine the quality of the products and clarify the causes of failure. Under equivalent conditions, the insulator iron cap, made of nodular graphite cast iron, failed when the load value reached 1929 kN by calculation, rather than 278 kN in this loading test. In this investigation, some of the defects were due to improper heat treatment process. When present, these defects eventually lead to fracture. The results of the research for the process design of insulator iron cap are available.

Keywords Insulator iron cap · HVDC · Failure · QT450 · Defect

Introduction

Electric energy has contributed greatly to the development of the modern economy. However, the safety of high-voltage transmission from remote areas to cities has been a topic of great concern [1]. An insulator is a significant component, widely used in the high-tension transmission field and it plays a vital role in supporting and fastening an energized conductor. It primarily consists of an iron cap, stalinite (or ceramics), as well as pin [2–4]. High tensile strength is required due to its working conditions [5–7]. If the parts of insulator have manufacturing defects which affect the tensile strength of materials, it could cause significant loss of property or personnel in engineering applications [8]. Therefore, it is necessary to ensure the quality of the insulator iron cap through adopting a reasonable process. In this case, an insulator was examined during a loading test [9], and an insulator cap, made of nodular graphite cast iron (QT450), fractured when the load reached 278 kN, far below the operating requirement. A schematic diagram and photographs of the insulator cap testing are shown in Fig. 1. The production process is as follows:

1. Fabricating of dry-core and casting blank;
2. Cleaning of sand, sprue and burr;
3. Casting in model, pickling with hydrochloric acid, galvanizing and detecting flows;
4. Pouring silicate cement into insulator cap and protecting in water at 70 °C.

According to the production process above, the micro-defects generated are likely to be related to the casting, pickling and galvanizing. During casting [10], some micro-defects are inevitable, such as gas porosity. In addition, these imperfections could link to each other to form crack sources under the load [11]. In order to obtain a better galvanizing effect, a pickling process is used to prepare the surface by removing contaminations, such as rust. However, porosity open to the surface could hold the pickling acid, allowing corrosion to occur, enlarging the potential defects [12]. For the galvanizing process, some defects would be generated, such as scratches [13]. In addition, the defects produced during galvanizing have an effect on the corrosion behavior and mechanical properties of the

X. Chen · S. Yan · C. Zhang (✉) · G. Cui · C. Yang
School of Material Science and Engineering, Southwest Jiaotong University, Chengdu 610031, China
e-mail: cszhang@swjtu.edu.cn

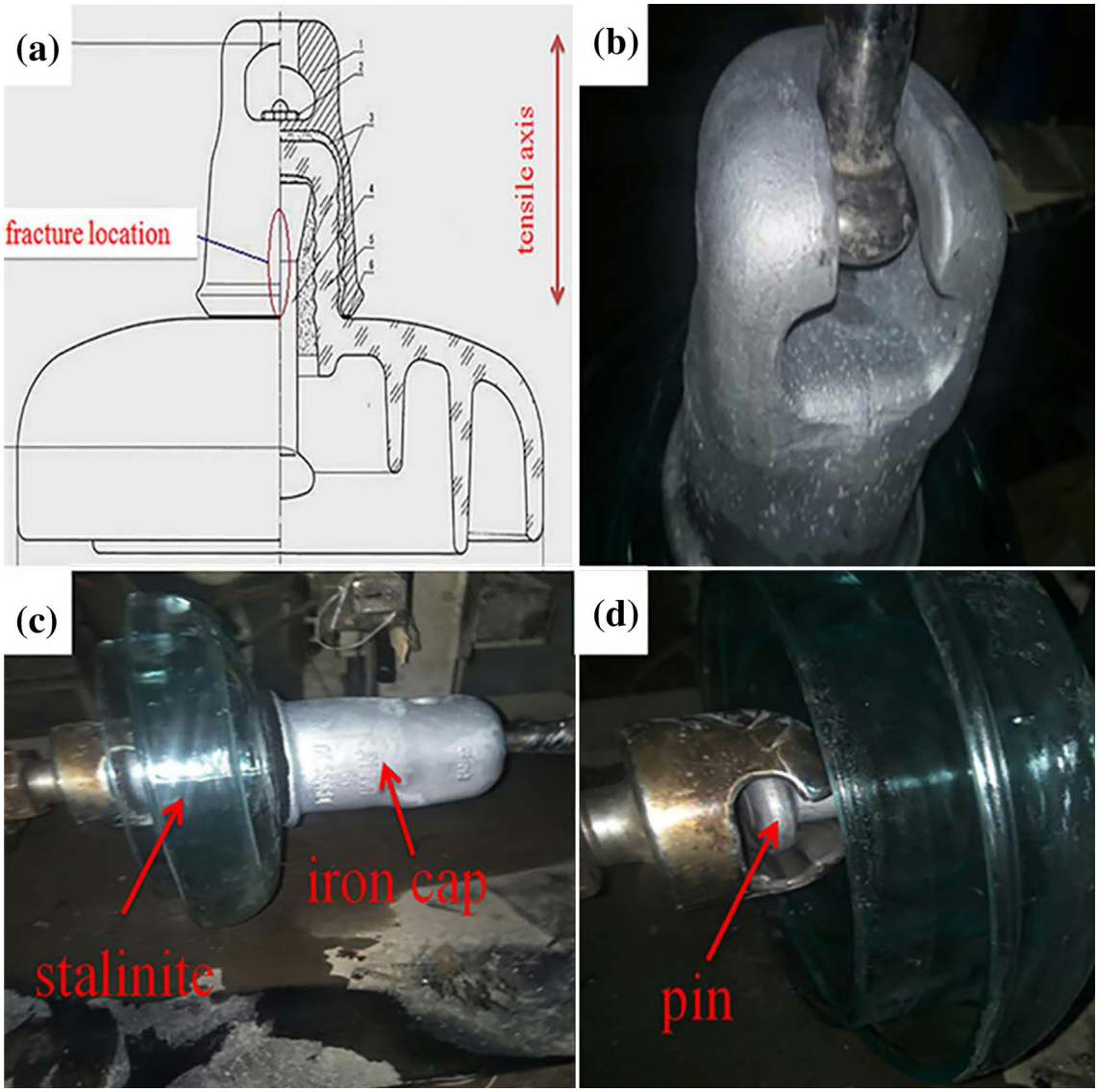

Fig. 1 Schematic diagram and actual photographs of the insulator cap testing: (**a**) sketch of insulator cap; (**b**), (**c**), (**d**) pictures of real product in loading test

material surface. In order to find the failure cause, an investigation was carried out in this case.

Experimental

The material used in this insulator iron cap was nodular graphite cast iron QT450 (C, 3.70–4.00%; Si, 2.15–2.93%; Mn, 0.46–0.66%; S, 0.010–0.016%; P, 0.027–0.035%; Mg, 0.027–0.050%; Re, 0.026–0.043%; Fe, balance). According to design criterion (GB/T 1348-2009), its tensile strength should be more than 450 MPa.

To investigate the main cause of the fracturing of the insulator iron cap and to make recommendations for manufacture, the procedure was to evaluate the failed components. Microstructures were observed using optical microscopy (Olympus GX51 optical microscope), and scanning electron microscopy (JSM-6490LV SEM), and the elements present were determined using energy-dispersive spectroscopy (EDS). The preparation of test samples required mechanical cutting, so that some oil contamination was left on the fracture surface. Therefore, in order to obtain more accurate results, the oil contamination on the fracture surface was cleaned carefully before analysis. Finally, the spherical rate of graphite was graded according to GB/T 9441-2009 and the maximum stress of insulator iron cap made of QT450 was calculated according to design criteria GB/T 1348-2009.

Results

Macroscopic Analysis

The macroscopic fractographs are shown in Fig. 2. It is indicated in Fig. 2a and b that the axis of the insulator cap is nearly parallel to the direction of tensile loading, and perpendicular to the fracture plane, suggesting this component failed due to tensile stress. In addition, the fracture position is located in the arc transition area, which is 75–80 mm from the top of the insulator cap. In Fig. 2c, two types of fracture areas were observed. One was a shining and smooth area, marked as Area 1, whose small crystalline particles are clearly visible. The other one was the jagged area, marked as Area 2. In addition, in Area 2, not only are there gray regions, but also partly blue and yellow regions. It is more notable from Fig. 2c that the rust line is exactly located at the junction of two kinds of areas, as well as the crack source at the tip of junction. Such rust was not found in the Area 1, suggesting the rust had possibly existed before loading test. Figure 2d shows a fragment from Area 2 after loading test, and there is a long crack in it. The tensile stress of the QT450 was calculated as follows, according to the material design criterion (assuming the stress of material is uniform everywhere).

R_1—small circle radius.
R_2—great circle radius.
F_m—maximum stress value.
σ_b—tensile strength of material.

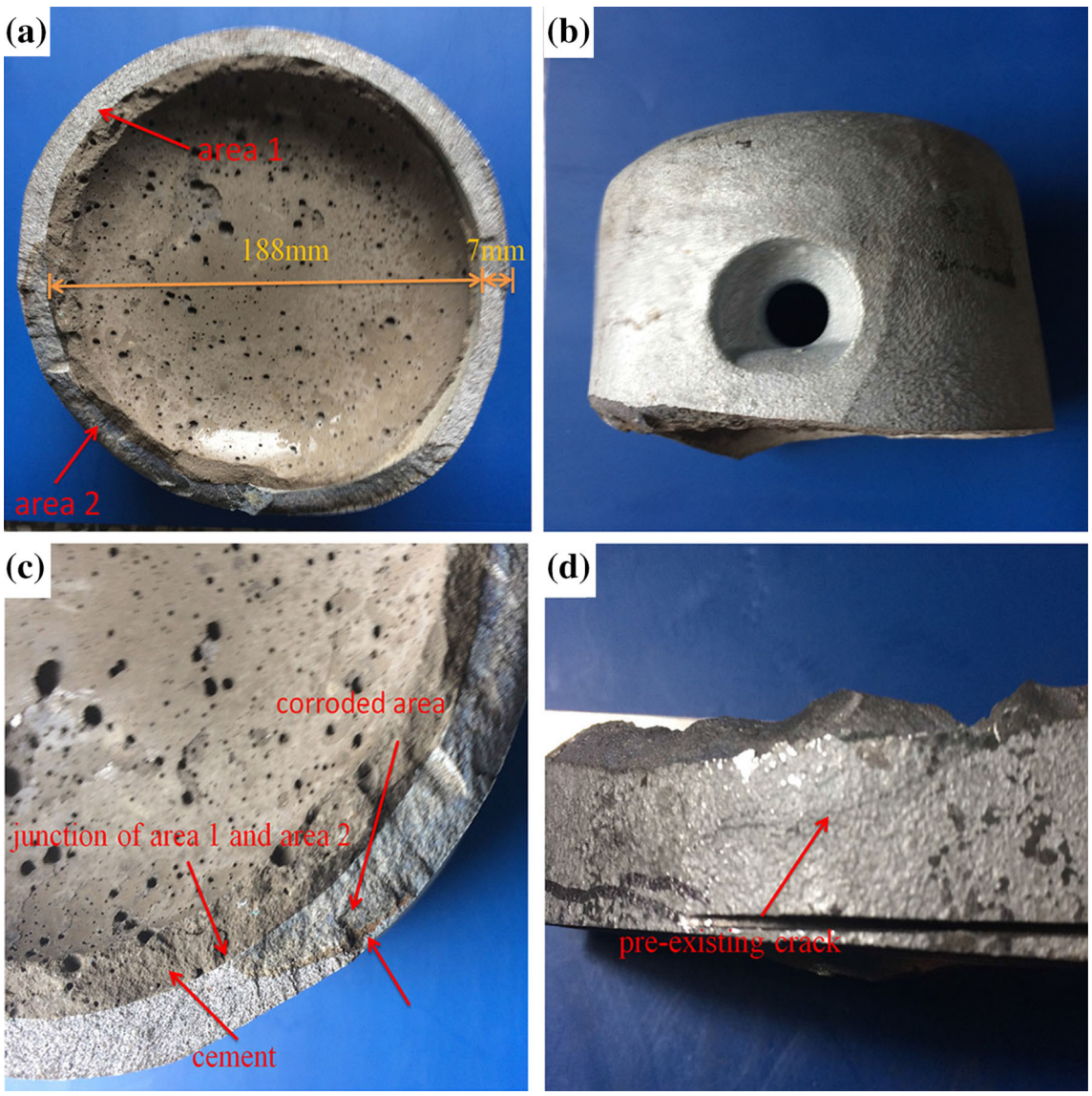

Fig. 2 Macrographs of fracture location: (**a**) complete fracture plane, (**b**) section of fracture plane, (**c**) the junction of Area 1 and Area 2, (**d**) a fragment from Area 2 after loading test

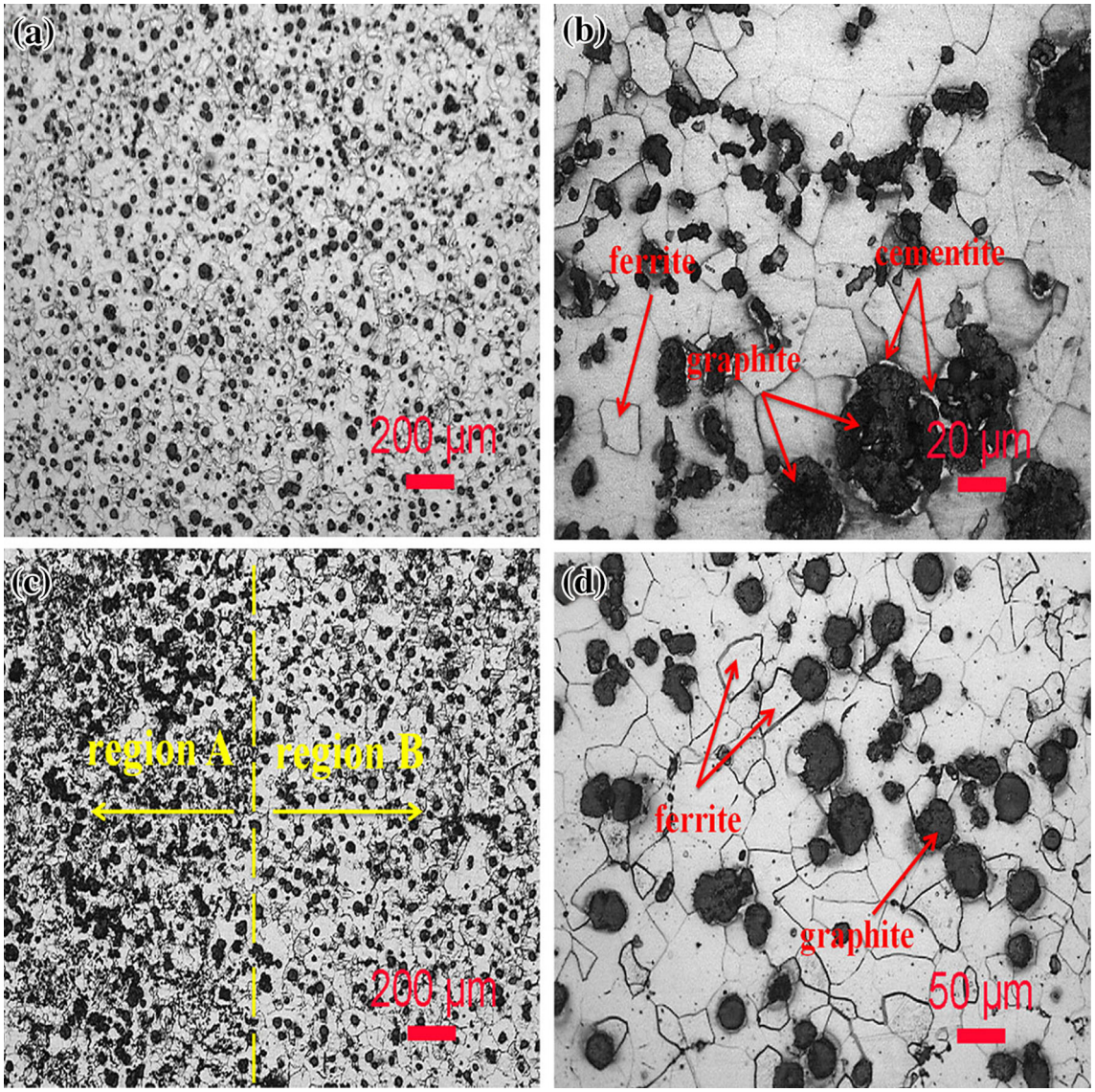

Fig. 3 Photomicrographs from the optical microscope, (**a**) and (**d**) transverse cross section; (**c**) and (**d**) longitudinal cross section

Insulator iron cap: $R_1 = 94$ mm, $R_2 = 101$ mm, $\sigma_b = 450$ MPa.

$A = (\pi R_2^2) - (\pi R_1^2) = \pi(R_2^2 - R_1^2) = 3.14 \times (101^2 - 94^2) = 4286\ \text{mm}^2$.

$F_m = A \times \sigma_b = 4286 \times 450 = 1929$ kN.

Therefore, according to the calculated result above, the insulator iron cap should not fail when the tensile stress reached 278 kN, indicating various defects existed into material.

Microstructure Analysis

Figure 3 shows the transverse and longitudinal micrographs obtained by optical microscope. The transverse plane is perpendicular to tensile axis, while the longitudinal

Table 1 Evaluation standard of spherical rate and size of graphite in QT450

Level	Average spherical rate of graphite (%)	Average size of graphite (mm)
1	≥ 95	…
2	90–95	…
3	80–90	> 0.25–0.5
4	70–80	> 0.12–0.25
5	60–70	> 0.06–0.12
6	50–60	> 0.03–0.06
7	…	> 0.015–0.03
8	…	≤ 0.015

Table 2 Evaluation result of samples

	Size (level)	Spherical rate (level)
Transverse	4	3
Longitudinal	5	3

plane is parallel to it. The microstructure of this fracture was mainly composed of ferrite, graphite, as well as bulk cementite distributed around the graphite. It is clear from Fig. 3c that an interface divided image into region A and B. And, the graphite was reunited in region A, in which the size and distribution of graphite were uneven. The size and

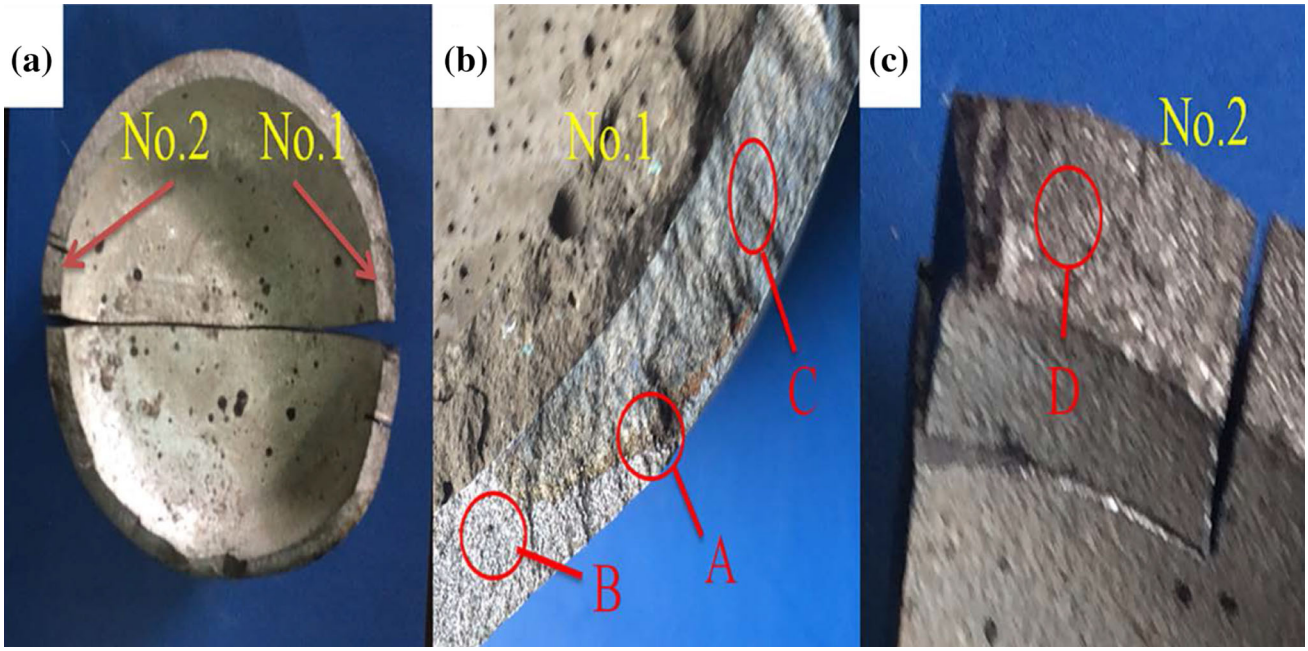

Fig. 4 The selected positions of SEM samples: (**a**) position of No. 1 and No. 2 samples on the fracture surface; (**b**) Areas A, B and C selected in No. 1 sample; (**c**) Area D selected in No. 2 sample

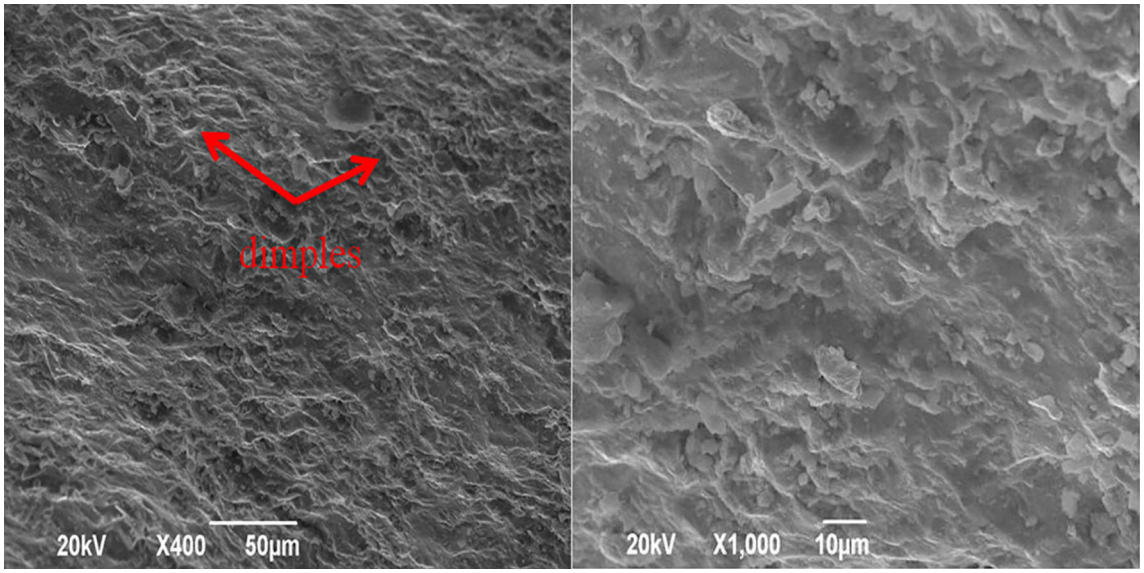

Fig. 5 SEM photomicrograph of No. 1 sample in Area B

spherical rate of graphite were evaluated according to GB/T 9441-2009, and the detailed evaluation standard and result were listed in Tables 1 and 2 respectively.

Figure 4 shows the SEM images of fracture surface of selected samples (No. 1 and No. 2). The Sample No. 1 included Rusted Area A, smooth fracture in Area B and Non-Rusted Area C. In addition, Areas A and C were located in the jagged fracture. Area B was normal plastic fracture because of dimples found in the Fig. 5. In case of Area A (see Fig. 6), the cleavage fracture feature was observed, suggesting a brittle fracture occurred in Area A. In addition, some granular particles were found. The EDS result of these particles in Fig. 6 showed that the content of carbon was 79.07 at.%, and much higher than that in ferrite (2.73 at.%). In addition, the elements, such as oxygen, aluminum, chlorine, calcium and zinc, were not the compositions of QT450. Instead, these elements were from the cement, hydrochloric acid, and galvanization. Among them, the discovery of chlorine element showed that a corrosion ever occurred in Area A, resulting in expanding

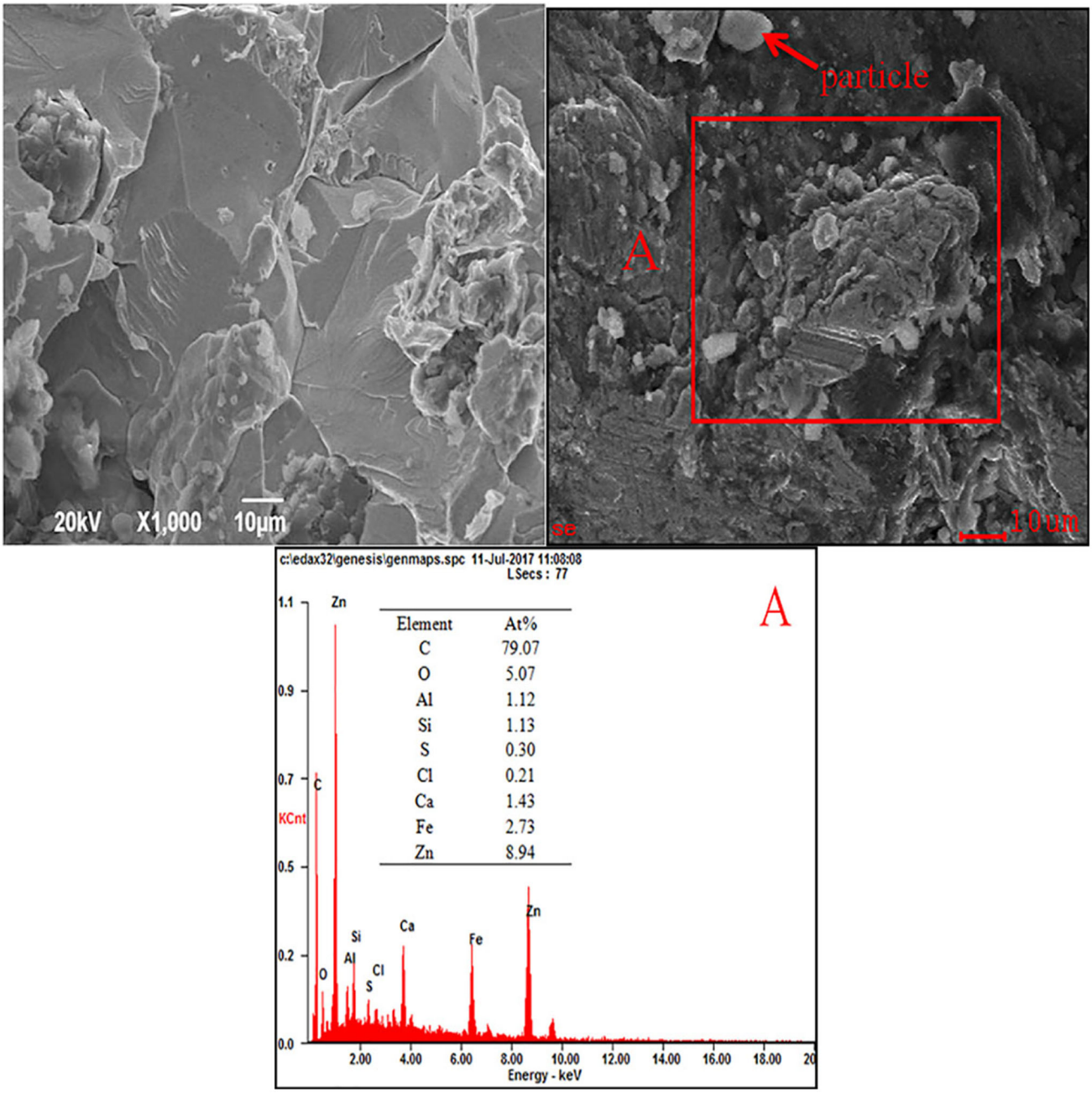

Fig. 6 SEM photomicrographs and EDS spectra of No. 1 sample in Area A

the size of the defects. Then, a large amount of zinc had already penetrated into it, before tensile loading test. In Fig. 7, the cleavage fracture feature contained a small amount of zinc was found. In Fig. 8, Area D included a graphite enrichment region, brittle fracture, as well as cement regions, marked as regions D1, D2 and D3, respectively. It was obvious in Fig. 8 that the content of carbon in D1 exceeded that in ferrite. In region D2, the cleavage brittle feature was observed too, and a small quantity of zinc was examined. The cement was located in region D3. In addition to the basic elements consisting of cement, the content of zinc increased obviously comparing with region D2. And, region D3 was originally a corrosion pit, but the non-solidified cement filled it in after pouring. Then, non-solidified cement mixed with zinc on the insulator iron cap surface, resulting in the content of zinc increase.

Discussion

According to various experimental results above, it could be affirmed that graphite in material had a serious local agglomeration, causing the size and distribution of graphite to be uneven. The graphite itself was a brittle phase and agglomeration of it leads to an increase in partial brittleness. In addition, both the surface and inside of this insulator iron cap contained plentiful micro-defects, so that

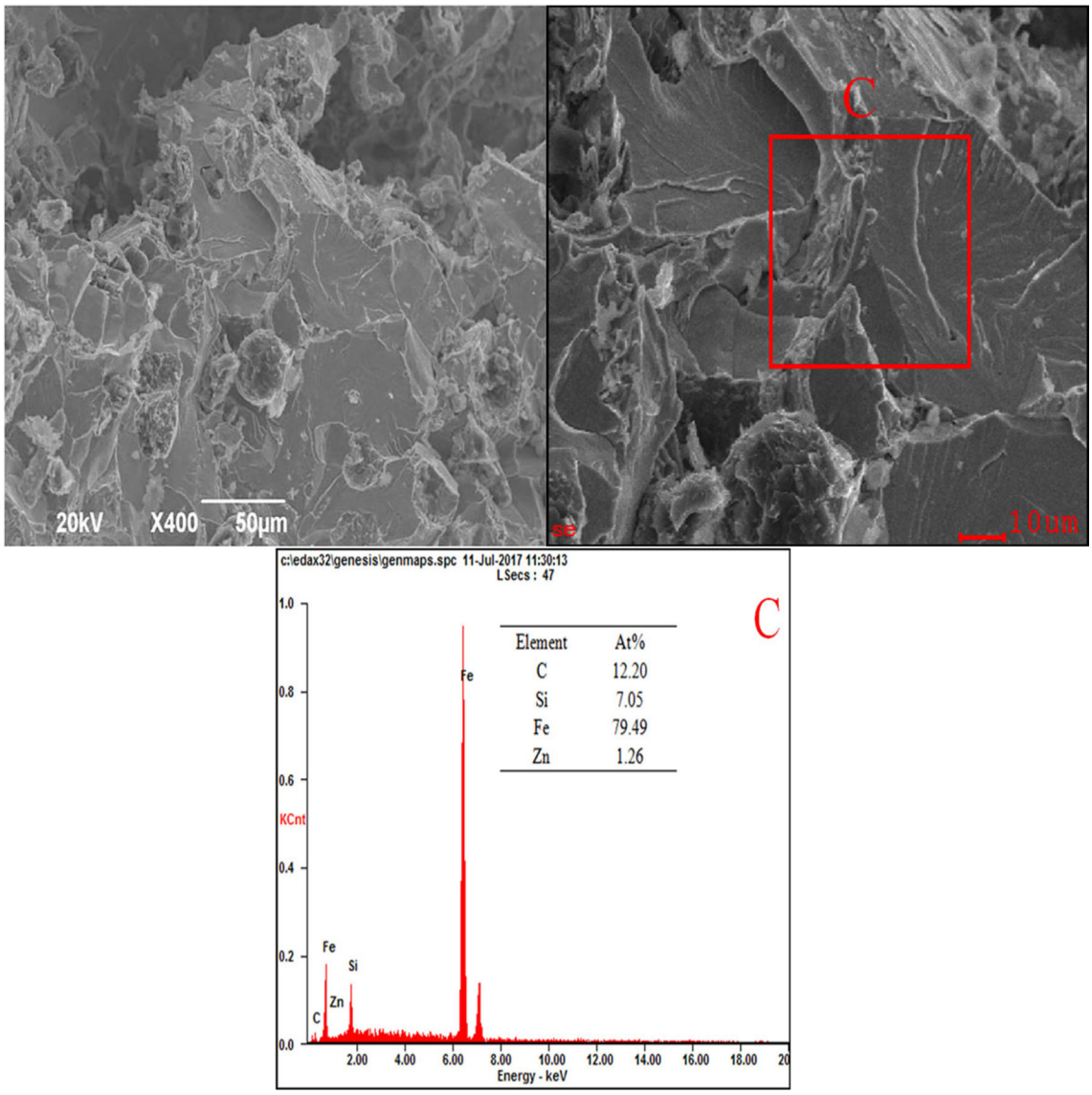

Fig. 7 SEM photomicrographs and EDS spectra of No. 1 sample in Area C

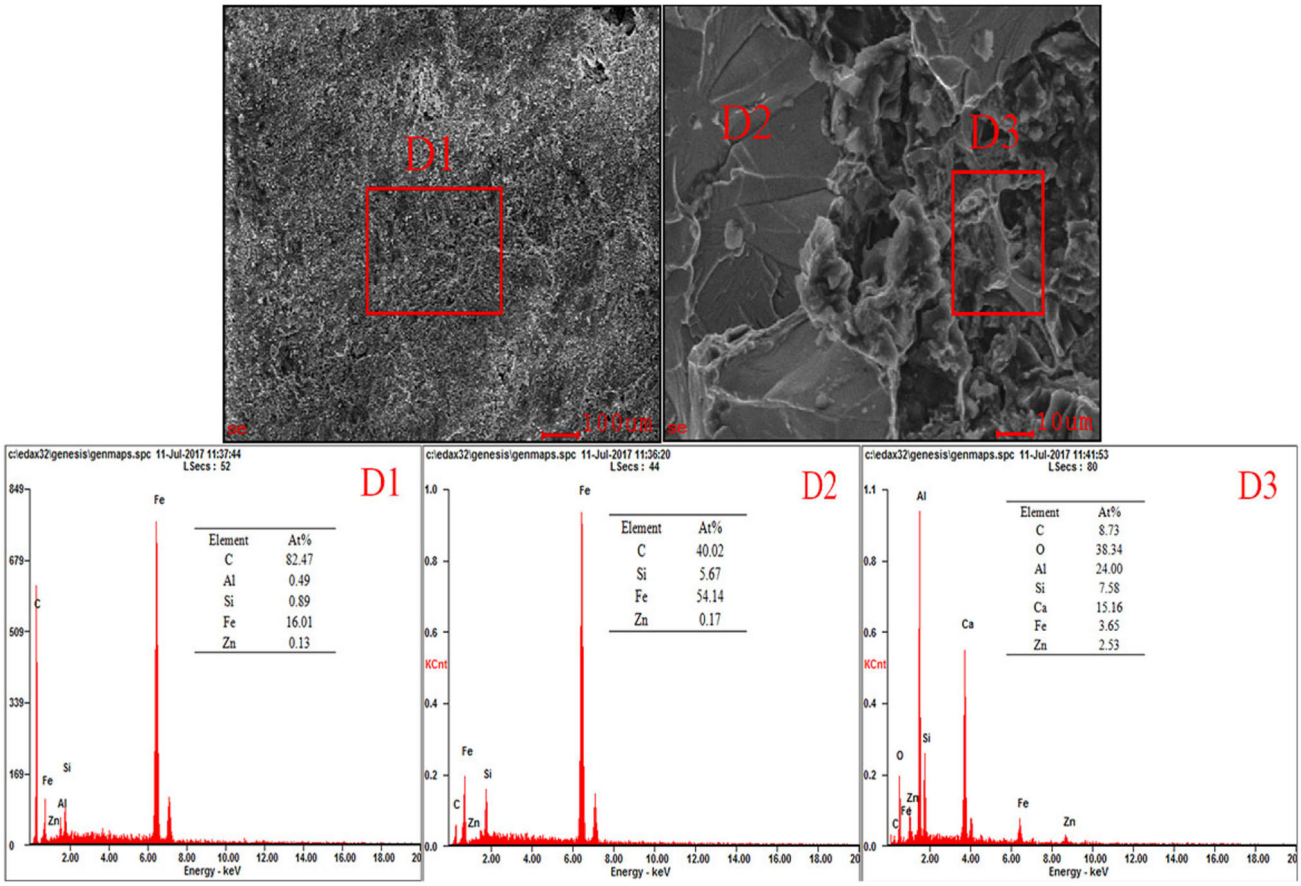

Fig. 8 SEM photomicrographs and EDS spectra of No. 2 sample in Area D: (D1) graphite-rich Area; (D2) QT450 substrate; (D3) cement connecting with insulator iron cap

the acid lotion could penetrate into the substrate along these micro-defects. Both the agglomeration of graphite and the formation of micro-defects were the result of improper casting process. Although the introduction of zinc also caused an increase in brittleness, the content of zinc in the substrate was relatively low and its influence on brittleness was limited. The brittle fracture of the substrate was mostly affected by agglomeration of graphite and the observed defects. Normal fracture should present plastic feature (see Fig. 7), instead of a brittle cleavage fracture. So, the fracture mechanism of this failure insulator iron cap was as follows:

1. Micro-defects, such as pores and cracks, were generated, and the graphite was reunited locally because of improper casting process.
2. During pickling, hydrochloric acid was able to penetrate into these pores and cracks on the surface, and initiate corrosion, directly resulting in expanding of these defects. In addition, hydrochloric acid was able to deeply penetrate into the body, leading to the rust line formation (see Fig. 4b).
3. For Area 2, all these adverse factors weakened the body's ability to withstand stress. These pre-cracks were continuously propagated under the loading, and the low-stress brittle fracture occurred when it reached the graphite enrichment region.

There were two main causes generating micro-porosities and cracks. The first one was that the graphite in the material could not diffuse evenly so it affected its plastic performance, if casting and holding time were not enough. During cooling, the first place to solidify was the outermost surface of material, which had the fastest cooling rate. If the cooling rate was too fast, the porosities existing inside the material would not be expelled and would eventually be retained in material. So, the effective way to reduce the porosities and make graphite homogenous distribution was to properly increase casting temperature, prolong holding time and decrease cooling rate.

Conclusion

In this investigation, the initial crack source was the rust line, derived from the micro-porosities and micro-cracks produced during casting and pickling. The body was stressed twice, propagating the initial cracks. The first was corroded by pickling solution, leading to the increase in crack size. The other was that after pickling, the expanded crack source continued propagating under loading stress. Since the graphite was brittle and reunited in some regions, it did not impede the expansion of the crack sources. When the crack propagated to the graphite enrichment area and the loading stress reached a certain value far below requirement, the area with more defects was prior to fracture.

Acknowledgments This work was supported by the National Natural Science Foundation of China (Grant Nos. 51601156 and U1537201) and Fundamental Research Funds for the Central Universities of China (Grant No. 2682016CX067).

References

1. A. Kalair, N. Abas, N. Khan, Comparative study of HVAC and HVDC transmission systems. Renew Sustain Energy Rev **59**, 1653–1675 (2016)
2. C.R. Bayliss, B.J. Hardy (eds.), Chapter 6: Insulators, in *Transmission and Distribution Electrical Engineering*, 4th edn. (Elsevier, Oxford, 2012), pp. 171–188
3. A.R. Verma, B.S. Reddy, Accelerated aging studies of silicon-rubber based polymeric insulators used for HV transmission lines. J. Polym. Test. **62**, 124–131 (2017)
4. P.S.R. Murty (ed.), Chapter 4: Insulators, in *Electrical Power Systems* (Elsevier, Oxford, 2017), pp. 61–75
5. Y. Zou, C. Gaudillere, J.E. Escribano et al., Microstructure, mechanical behavior and flow resistance of freeze-cast porous 3YSZ substrates for membrane applications. J Eur Ceram Soc **37**, 3167–3176 (2017)
6. J.E. Contreras, E.A. Rodriguez, Nanostructured insulators—a review of nanotechnology concepts for outdoor ceramic insulators. J. Ceram. Int. **43**, 8545–8550 (2017)
7. N. Clayton, M. Crouchen, A. Devred, D. Evans et al., Manufacture and mechanical characterisation of high voltage insulation for superconducting busbars—(Part 1) materials selection and development. J. Cryog. **83**, 64–70 (2017)
8. X. Xiaohong, Z. Tang, W. Jianfeng et al., Preparation and freeze-thaw resistance of alumina based ceramic insulators for extremely cold areas. J. Ceram. Int. **43**, 2712–2719 (2017)
9. ISO6892-1:2006, *Metallic Materials—Tensile Testing—Part 1: Method of Test at Room Temperature* (ISO, Geneva, 2006)
10. A. George, Pantazopoulos, failure and fracture analysis of a Zn-alloy casting. J Fail Anal Prev **17**, 400–406 (2017)
11. E.E. Vernon, M.E. Stevenson, J.L. McDougall, L. McCall, Failure analysis of gray iron pump housings. J. Fract. Anal. Prev. **4**, 15–18 (2004)
12. A. Mucsi, Analysis of coil break defects. J. Eng. Fail. Anal. **83**, 109–116 (2018)
13. A. Azimi, F. Ashrafizadeh, M.R. Toroghinejad, F. Shahriari, Metallurgical assessment of critical defects in continuous hot dip galvanized steel sheets. J. Surf. Coat. Technol. **206**, 4376–4383 (2012)